



Cite this: *New J. Chem.*, 2021, **45**, 3387

Received 23rd December 2020,
 Accepted 27th January 2021

DOI: 10.1039/d0nj06230h

rsc.li/njc

High electron transfer of TiO₂ nanorod@carbon layer supported flower-like WS₂ nanosheets for triiodide electrocatalytic reduction†

Wei Wang,^{‡*} Tianyu Liu,[‡] Chuan Ding,^a Min Wang,^a Jirong Bai,^a Jintao Zhang,^a Hengchang Bi,^{*c} Yueming Sun^d and Yuqiao Wang^{‡*}

WS₂-based nanomaterials have been extensively studied due to their unique catalytic properties. However, it is still a great challenge to prepare WS₂-based electrocatalysts with both maximally active edge sites exposure and high electronic conductivity. In this work, we have engineered a 1D–2D multidimensional nanostructured TiO₂ nanorod@carbon layer supported flower-like WS₂ nanosheets (TNRs@C@WS₂) electrocatalyst with abundant exposed active edge sites as well as high electron transfer abilities. The TNRs@C@WS₂ was explored as a good catalyst for the triiodide reduction reaction. The assembled dye-sensitized solar cell achieves a high photoelectric conversion efficiency (7.15%) and comparable to that (7.18%) of Pt. This unique 1D–2D multidimensional nanostructure may open up new opportunities for a variety of applications in clean energy and catalysis.

Introduction

Layered transition metal dichalcogenide (TMD) materials have gained a great deal of attention owing to their intriguing catalytic properties.^{1–4} Layered TMDs have strong covalent bonds in plane and weak van der Waals interactions between the adjacent layers to form a bulk crystal.⁵ The weak interlayer interactions enable the exfoliation of the layered TMDs into single- or few-layer two-dimensional (2D) nanosheets (NSs) with unique catalytic properties.^{6–9} Specifically, 2D MS₂ (M = Mo, W)

NSs have been demonstrated to be promising replacements for Pt-based catalysts toward electrocatalytic reactions, such as the hydrogen evolution reaction (HER) and the triiodide reduction reaction (IRR), due to their high electrocatalytic activity, excellent chemical stability, and cost-effectiveness.^{10–17} However, it is generally believed that the electrocatalytic activity of 2D MS₂ NSs mainly arises from their edges.^{18–20} Additionally, the intrinsic low electronic conductivity of MS₂ has greatly limited its electrocatalytic reaction kinetics. In the last two decades, great efforts have been made to explore various forms of MS₂ nanomaterials for HER or IRR applications, where the guiding principle has most often been to expose the active edge sites or increase the electronic conductivity.^{21–26} For example, constructing vertically aligned NSs or defect-engineered NSs for maximally exposing the active edge sites, and growing MS₂ on carbon nanomaterials or other electronic conductive nano-substrates for reducing the charge transfer resistance.^{22,27–30} However, it is still a huge challenge to prepare WS₂-based catalysts with both maximally exposed active sites and high electron transfer capacities.

In this work, we have designed a 2D flower-like WS₂ nanosheets electrocatalyst, loaded on a one-dimensional (1D) TiO₂ nanorods@carbon layers (TNRs@C) nano-substrate (Fig. 1). The carbon layers coated 1D TNRs were realized by a simple hydrothermal method. The 1D TNRs@C supported 2D flower-like WS₂ nanosheets (TNRs@C@WS₂) were obtained *via* a chemical vapor deposition (CVD) process. The detailed synthetic methods and characterizations are given in the experimental section. The prepared 1D–2D multidimensional nanostructured TNRs@C@WS₂ was introduced as an effective catalyst for the IRR.

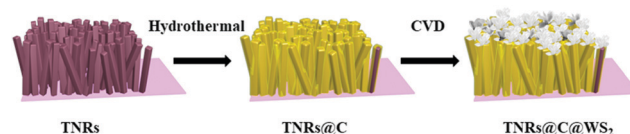


Fig. 1 The fabrication process for TNRs@C@WS₂.

^a School of Chemical Engineering and Materials, Changzhou Institute of Technology, Changzhou 213032, P. R. China. E-mail: mse_wwang@ntu.edu.sg

^b Center for Programmable Materials, School of Materials Science and Engineering, Nanyang Technological University, 50 Nanyang Avenue, Singapore 639798, Singapore

^c Shanghai Key Laboratory of Multidimensional Information Processing, School of Communication and Electronic Engineering, East China Normal University, Shanghai 200241, P. R. China. E-mail: hcbi@cee.ecnu.edu.cn

^d Institute of Advanced Materials, School of Chemistry and Chemical Engineering, Southeast University, Nanjing 211189, P. R. China. E-mail: yqwang@seu.edu.cn

† Electronic supplementary information (ESI) available. See DOI: 10.1039/d0nj06230h

‡ These authors contributed equally to this work.

The assembled dye-sensitized solar cell (DSSC) achieves a high photoelectric conversion efficiency (PCE) (7.15%), which is comparable to that (7.18%) of Pt.

Experimental

Fabrication of TNRs/C

Concentrated hydrochloric acid (40 mL) and titanium tetrachloride (400 μL) were added to distilled water (50 mL) and stirred for 25 min. The mixture and FTO substrates were placed inside the Teflon-coated autoclave. The autoclave was hydrothermally treated in an oven at 180 $^{\circ}\text{C}$ for 120 min and cooled down to room temperature naturally. Then, the 1D TNR samples were obtained. Glucose (~ 1 g) was mixed with 18 mL deionized water to form a homogeneous glucose solution. The glucose solution and TNRs were placed into the autoclave and kept at 180 $^{\circ}\text{C}$ for 4 h, after which the TNRs@C samples were obtained.

Fabrication of TNRs@C@WS₂

The TNRs@C sample was put into a mixture of ammonium tungstate ($(\text{NH}_4)_{10}\text{H}_2(\text{W}_2\text{O}_7)_6$) (99.99%, Macklin) and distilled water (150 mg mL^{-1}) for about 30 min. After air-drying, the TNRs@C@W-precursor and sulfur powder were put into a chemical vapor deposition (CVD) system. The procedure was ramped to 500 $^{\circ}\text{C}$ under N_2 (99.9%) flow at a rate of 10 $^{\circ}\text{C min}^{-1}$, and kept at 500 $^{\circ}\text{C}$ for 30 min, then cooled down naturally.

Fabrication of the DSSC device

The screen-printing method was used to synthesize the photoanode. TiO_2 photoanodes were sensitized by Ru-dyes N719 and coupled with one of the CEs (TNRs@C@WS₂ or Pt) to fabricate DSSCs. The electrolyte of iodide/triiodide was injected into the space between the photoanodes and CEs.

Material characterization and electrochemical measurements

Scanning electron microscopy (SEM, FEI) and transmission electron microscopy (TEM, JEM-2100) were used to characterize the morphologies of the samples. Raman spectra were recorded on a Horiba-JY HR 800 equipped with a 514.5 nm laser source. Cyclic voltammetry (CV) measurements were performed in the standard three-electrode system using a CHI760E electrochemical workstation. Ag/AgCl and a platinum wire were used as the reference electrode and counter electrode, respectively. 10 mM LiI, 0.1 M LiClO_4 , and 1 mM I_2 were mixed in acetonitrile and employed as an electrolyte. Current-voltage (I - V) characteristics of the CEs were obtained using a Keithley 2400 under Newport Oriol 91.192 simulated illumination in the dark and under AM1.5, 100 mW cm^{-2} . The EIS tests were measured at open circuit potential in the frequency range from 0.01 to 10^5 Hz with a perturbation amplitude of 5 mV.

Results and discussion

Structure and morphology

The SEM and TEM techniques were employed to study the nanostructure of the TNRs and TNRs@C. The SEM images of the TNRs are shown in Fig. S1a in the ESI[†]. The 1D nanorods are vertically aligned to the FTO substrate. The average diameter of the nanorods is about 80 nm, and the mean height of the nanorods is about 800 nm (Fig. S1a, ESI[†]). The SEM image of TNRs@C is shown in Fig. S1b (ESI[†]), and the TNRs@C also exhibits a nanorod-like morphology. Moreover, this unique 1D nanostructure is beneficial for the electron and electrolyte ion transport during the electrocatalytic reaction. The elemental distribution of the TNRs@C was analyzed by elemental mapping (Fig. S1d-f, ESI[†]). The results demonstrate that C, O, and Ti are presented and evenly distributed in the TNR nano-substrate. TNRs@C was also investigated by transmission electron microscopy (TEM). As shown in Fig. S1j and h (ESI[†]) the thickness of the carbon nanofilm layer is about 3 nm.

The morphology of the as-designed 1D-2D multidimensional TNRs@C@WS₂ was studied by SEM and TEM. The flower-like WS₂ is made up of 2D edge-oriented thin WS₂ nanosheets, growing on top of 1D TNRs@C, and the average diameter of flower-like WS₂ is ~ 800 nm (Fig. 2a and b). These particular flower-like WS₂ nanostructures ensured that the

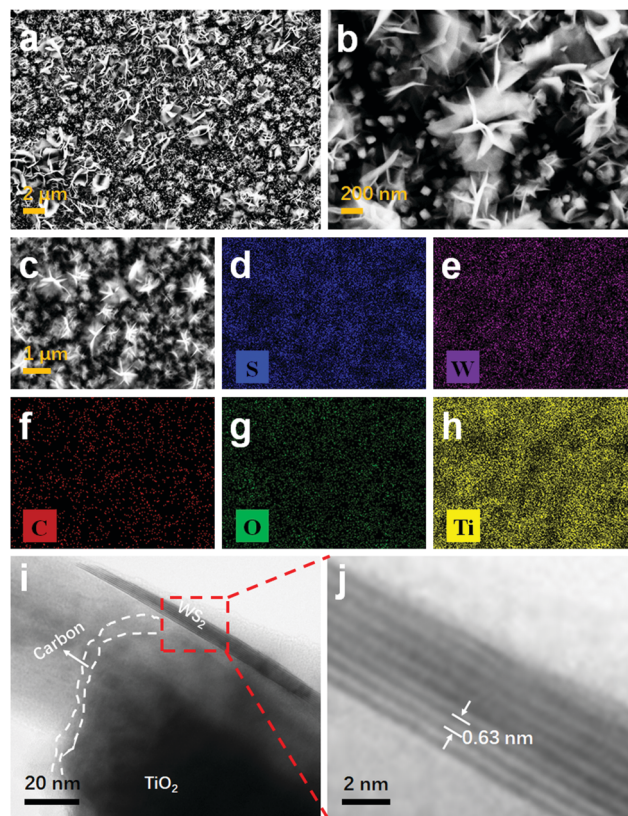


Fig. 2 (a and b) SEM images of the TNRs@C@WS₂. (c) STEM image and EDS elemental mapping of (d) sulphur, (e) tungsten, (f) carbon, (g) oxygen and (h) titanium elements in TNRs@C@WS₂. (i) TEM and (j) HR-TEM images of TNRs@C@WS₂.

exposure of abundant edge sites of TNRs@C@WS₂ was performed using SEM. The elements of S, W, C, O, and Ti are detected in the 1D–2D multidimensional nanostructured TNRs@C@WS₂ by EDS elemental mapping under scanning transmission electron microscopy (STEM) (Fig. 2c–h). The TEM image of TNRs@C@WS₂ shows that the WS₂ nanosheet is tightly attached to the 1D TNRs/C nano-substrate (Fig. 2i). The thickness of the WS₂ nanosheet is ~5 nm (about 8 layers). By high-resolution TEM (HR-TEM), lattice fringes of the WS₂ nanosheet are clearly observed, suggesting that the obtained WS₂ nanosheet has a good crystallinity (Fig. 2j). WS₂ shows a lattice fringe, corresponding to the (002) plane of 2H-WS₂, which is about 0.63 nm. These results demonstrate that TNRs@C@WS₂ is composed of 1D TNRs coated with a conductive carbon layer for efficient electron and electrolyte ion transport, and 2D edge-oriented WS₂ nanosheets provide plenty of exposed active edge sites. In view of fast electron and electrolyte ion transport, as well as abundant exposed active edge sites, the 1D–2D multidimensional nanostructured TNRs@C@WS₂ is believed to act as a high performance electrocatalyst.

Fig. 3a displays the Raman spectra of different materials. The Raman spectrum of TNRs shows peaks at ~239.9 (two-phonon scattering mode), ~446.3 (E_g mode) and ~610.3 (A_{1g} mode) cm⁻¹, indicating the rutile phase.^{31,32} However, compared with TNRs, the TNRs/C reveals two other peaks at ~1372.2 and ~1595.3 cm⁻¹. These two peaks are assignable to the D-band (~1372.2 cm⁻¹) and G-band (~1595.3 cm⁻¹) of carbon. Apparently, TNRs@C@WS₂ displays two more peaks, corresponding to E_{12g} (~348.5 cm⁻¹) and A_{1g}¹ (~413.2 cm⁻¹) modes of WS₂, respectively. In addition, the chemical composition of the TNRs@C@WS₂ was collected using EDS. The EDS spectrum displays that S, W, C, O, and Ti exist in the 1D–2D multidimensional nanostructured material, which agrees well with the elemental mapping results. This further confirms the results of Raman (Fig. 3b).

Electrochemical properties of TNRs@C@WS₂

The TNRs@C@WS₂ was exploited to fabricate a DSSC as a CE. The catalytic activities of the CEs were evaluated by CV analyses (Fig. 4a). Two pairs of obvious redox peaks can be clearly observed for the Pt based CE, revealing the high electrocatalytic activity of the Pt CE towards the IRR. The peak shapes and positions of the TNRs@C@WS₂ CE are similar to those of Pt

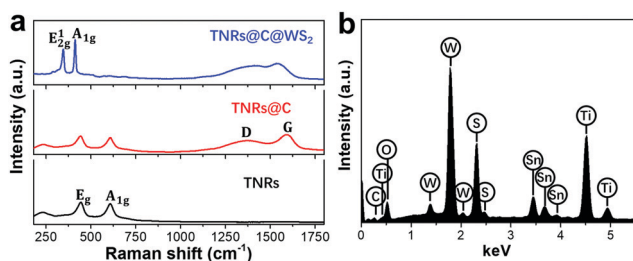


Fig. 3 (a) Raman spectra of TNRs, TNRs@C, and TNRs@C@WS₂. (b) The EDS spectrum of TNRs@C@WS₂. The Sn signals come from the FTO substrate.

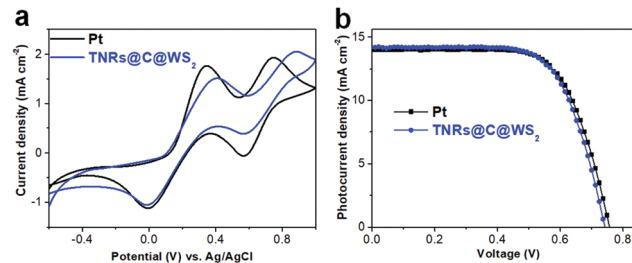


Fig. 4 (a) CV curves using TNRs@C@WS₂ and Pt as CEs for the iodide/triiodide redox couple in the electrolyte at a scan rate of 50 mV s⁻¹. (b) *I*–*V* curves of DSSCs using TNRs@C@WS₂ and Pt as CEs.

CE, indicating the high electrocatalytic activity of the TNRs@C@WS₂. In order to understand the charge-transfer mechanism, the CV performances of the TNRs@C@WS₂ CE at various scan rates were measured. As shown in Fig. S2a (ESI[†]), the peak current densities increased with increasing scanning rates, and linear relationships between the peak currents and square roots of scan rate are observed (Fig. S2b, ESI[†]). This result indicates that the electrochemical reaction on the TNRs@C@WS₂ CE is a diffusion-controlled process.^{33–36}

Meanwhile, the *I*–*V* curves of the DSSCs using Pt and TNRs@C@WS₂ CEs are exhibited in Fig. 4b, and detailed photovoltaic parameters of the DSSCs are collected (Table 1). TNRs@C@WS₂ CE displayed a PCE of 7.15%, which is very close to that (7.18%) of the Pt CE. This high PCE can be mainly attributed to the unique 1D–2D multidimensional nanostructure of TNRs@C@WS₂ which possesses not only a large amount of exposed active edge sites but also a small charge transfer resistance. Additionally, the photovoltaic parameters for the DSSCs with different MS₂-based CEs are displayed in Table 2. The PCE (7.15%) of the TNRs@C@WS₂ based DSSC is among the best of other MS₂-based DSSC devices, indicating excellent electrocatalytic activity of TNRs@C@WS₂ toward the IRR.

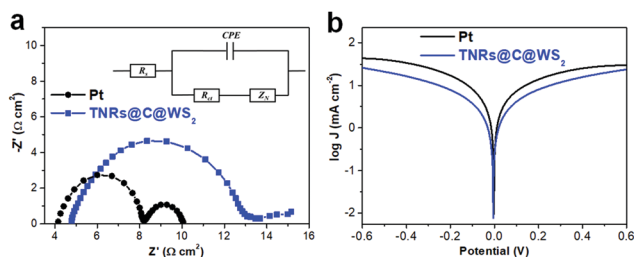
EIS experiments were used to elucidate the electron transport behavior and further evaluate the electrocatalytic activities of the Pt and TNRs@C@WS₂ CEs. Fig. 5a shows the Nyquist plots of the dummy cells, and the corresponding EIS parameters were obtained by the Z-view software (Table 1). The *R*_s value of TNRs@C@WS₂ (4.326 Ω cm²) was comparable to that of Pt (3.985 Ω cm²), suggesting a good bonding strength between the FTO substrate and the nanostructured TNRs@C@WS₂, which in turn promotes the transfer of holes from the electrolyte or of electrons from the external circuit to the CE.³⁷ The semicircle at the high-frequency region corresponds to the charge-transfer resistance (*R*_{ct}) at the electrolyte–electrode interface.^{38–43} In addition, the low *R*_{ct} usually points to the high

Table 1 Photovoltaic and EIS parameters of DSSCs with different CEs

CEs	<i>J</i> _{sc} (mA cm ⁻²)	<i>V</i> _{oc} (V)	FF	PCE (%)	<i>R</i> _s (Ω cm ²)	<i>R</i> _{ct} (Ω cm ²)
Pt	13.9	0.758	0.68	7.18	3.985	4.261
TNRs@C@WS ₂	14.2	0.743	0.68	7.15	4.326	9.352

Table 2 Photovoltaic parameters for the DSSCs with different MS₂-based CEs

CEs	J_{sc} (mA cm ⁻²)	V_{oc} (V)	FF	PCE (%)	Ref.
TiO ₂ -WS ₂	13.43	0.71	0.66	6.3	44
1T MoS ₂	18.76	0.73	0.52	7.08	14
G-MoS ₂	16.1	0.66	0.67	7.1	45
TNAs@FL-MoS ₂	14.45	0.751	0.66	7.16	46
WS ₂ /MWCNT	13.63	0.75	0.72	7.36	23
W-N/C@Co ₉ S ₈ @WS ₂	15.74	0.72	0.65	7.38	47
TNRs@C@WS ₂	14.2	0.743	0.68	7.15	This work

**Fig. 5** (a) Nyquist plots and (b) Tafel polarization curves of DSSCs using TNRs@C@WS₂ and Pt as CEs.

electrocatalytic activity of the CE, resulting in the acceleration of the high electron-transfer process at the electrolyte/CE interface. The low R_{ct} values of TNRs@C@WS₂ CE (9.352 Ω cm²) and Pt (4.261 Ω cm²) suggest the low electron transport resistances as well as good electrocatalytic activities of the electrocatalysts for the IRR. Tafel polarization was also carried out to elucidate the electrocatalytic activity of the CEs for DSSCs. The Tafel polarization curves for the TNRs@C@WS₂ and Pt CEs are displayed in Fig. 5b. The TNRs@C@WS₂ shows an exchange current density (J_0) value assimilable to that of the Pt CE. This also means that TNRs@C@WS₂ has a good electrocatalytic activity for the IRR. These results provide further support for the analysis of CV, IV, and EIS measurements.

In addition to the high electrocatalytic activity, TNRs@C@WS₂ also has outstanding durability toward the IRR. Fig. S3 (ESI[†]) exhibits the stability of TNRs@C@WS₂. CV analysis was carried out to evaluate the electrochemical stability of the TNRs@C@WS₂ CE (Fig. S3a, ESI[†]). The TNRs@C@WS₂ CE exhibits no remarkable change after 20 consecutive voltammetric cycles. Furthermore, the long-term stability of the DSSC with the TNRs@C@WS₂ CE was also analyzed (Fig. S3b, ESI[†]). The value of PCE is found to be only slightly decreased relative to the initial value (from 7.15% to 6.95%) after being stored for 20 days under ambient conditions, suggesting its good long-term stability.

Conclusions

In summary, we have achieved a 1D–2D multidimensional nanostructured TNRs@C@WS₂ consisting of 1D TNRs@C nanorods and 2D flower-like edge-oriented WS₂ nanosheets. 1D TNRs@C nanorods allowed for highly efficient electron and electrolyte ion transport, while the 2D edge-oriented WS₂

nanosheets guaranteed the abundant active edge sites. Thus, this unique 1D–2D multidimensional nanostructured TNRs@C@WS₂ ensures sufficient catalytic activity for electrocatalytic reactions. TNRs@C@WS₂ was determined as a good electrocatalyst for the IRR in a DSSC, exhibiting a high PCE of 7.15%, which is among the best of the MS₂-based CEs and comparable to that of (7.18%) the Pt CE, owing to its high electron transportability as well as the abundant exposed active edge sites of the nanomaterials. In addition, the WS₂ based 1D–2D multidimensional nanostructured materials with both good electronic conductivity and high electrocatalytic activity show promising potential for applications in high-performance electrocatalysis.

Author contributions

Wang W., Bi H. and Wang Y. designed and engineered the experiments; Wang W. and Liu T. synthesized and characterized the samples; Wang W., Liu T., Ding C., Wang M., Bai J. and Zhang J. contributed to the data analysis; Wang W. prepared the manuscript with support from Bi H., Sun Y. and Wang Y. All authors contributed to the general discussion.

Conflicts of interest

The authors declare that they have no conflicts of interest.

Acknowledgements

This work was financially supported by the Natural Science Foundation of China (61774033, 52002038), the Natural Science Foundation of Jiangsu (BK20170661), and the Science and Technology Project of Changzhou (CJ20200037). This work was also supported by the Engineering Research Center for Nanophotonics & Advanced Instrument, Ministry of Education, East China Normal University.

References

- Z. Lin, Y. Liu, U. Halim, M. Ding, Y. Liu, Y. Wang, C. Jia, P. Chen, X. Duan, C. Wang, F. Song, M. Li, C. Wan, Y. Huang and X. Duan, *Nature*, 2018, **562**, 254–258.
- Y. Chen, Z. Lai, X. Zhang, Z. Fan, Q. He, C. Tan and H. Zhang, *Nat. Rev. Chem.*, 2020, **4**, 243–256.
- X. Zhu, D. Li, X. Liang and W. D. Lu, *Nat. Mater.*, 2018, **18**, 141–148.
- S. Y. Xu, Q. Ma, Y. Gao, A. Kogar, A. Zong, A. M. Mier Valdivia, T. H. Dinh, S. M. Huang, B. Singh, C. H. Hsu, T. R. Chang, J. P. C. Ruff, K. Watanabe, T. Taniguchi, H. Lin, G. Karapetrov, D. Xiao, P. Jarillo-Herrero and N. Gedik, *Nature*, 2020, **578**, 545–549.
- R. Cheng, S. Jiang, Y. Chen, Y. Liu, N. Weiss, H. C. Cheng, H. Wu, Y. Huang and X. Duan, *Nat. Commun.*, 2014, **5**, 5143.
- Q. Peng and S. De, *Phys. Chem. Chem. Phys.*, 2013, **15**, 19427–19437.

- 7 H. Zhu, Y. Wang, J. Xiao, M. Liu, S. Xiong, Z. J. Wong, Z. Ye, Y. Ye, X. Yin and X. Zhang, *Nat. Nanotechnol.*, 2015, **10**, 151–155.
- 8 W. Wu, L. Wang, Y. Li, F. Zhang, L. Lin, S. Niu, D. Chenet, X. Zhang, Y. Hao, T. F. Heinz, J. Hone and Z. L. Wang, *Nature*, 2014, **514**, 470–474.
- 9 Y. Yin, J. Han, Y. Zhang, X. Zhang, P. Xu, Q. Yuan, L. Samad, X. Wang, Y. Wang, Z. Zhang, P. Zhang, X. Cao, B. Song and S. Jin, *J. Am. Chem. Soc.*, 2016, **138**, 7965–7972.
- 10 X. Sun, J. Dai, Y. Guo, C. Wu, F. Hu, J. Zhao, X. Zeng and Y. Xie, *Nanoscale*, 2014, **6**, 8359–8367.
- 11 C. Tan, Z. Lai and H. Zhang, *Adv. Mater.*, 2017, 29.
- 12 B. Chen, G. Sun, J. Wang, G. Liu, C. Tan, Y. Chen, H. Cheng, J. Chen, Q. Ma, L. Huang, P. Chen and H. Zhang, *Chem. Commun.*, 2020, **56**, 5131–5134.
- 13 C. Tan, W. Zhao, A. Chaturvedi, Z. Fei, Z. Zeng, J. Chen, Y. Huang, P. Ercius, Z. Luo, X. Qi, B. Chen, Z. Lai, B. Li, X. Zhang, J. Yang, Y. Zong, C. Jin, H. Zheng, C. Kloc and H. Zhang, *Small*, 2016, **12**, 1866–1874.
- 14 W. Wei, K. Sun and Y. H. Hu, *J. Mater. Chem. A*, 2016, **4**, 12398–12401.
- 15 W. Wang, H. Bi, C. Li, J. Zhang, J. Feng, Y. Wang, X. Huang, Y. Sun and L. Sun, *Mater. Today Nano*, 2019, **6**, 100033.
- 16 X. Xu, X. Tian, B. Sun, Z. Liang, H. Cui, J. Tian and M. Shao, *Appl. Catal., B*, 2020, **272**, 118984.
- 17 X. Xu, B. Sun, Z. Liang, H. Cui and J. Tian, *ACS Appl. Mater. Interfaces*, 2020, **12**, 26060–26067.
- 18 T. F. Jaramillo, K. P. Jørgensen, J. Bonde, J. H. Nielsen, S. Horch and I. Chorkendorff, *Science*, 2007, **317**, 100–102.
- 19 J. Xie, J. Zhang, S. Li, F. Grote, X. Zhang, H. Zhang, R. Wang, Y. Lei, B. Pan and Y. Xie, *J. Am. Chem. Soc.*, 2013, **135**, 17881–17888.
- 20 S. Yu, J. Kim, K. R. Yoon, J. W. Jung, J. Oh and I. D. Kim, *ACS Appl. Mater. Interfaces*, 2015, **7**, 28116–28121.
- 21 M. R. Gao, M. K. Chan and Y. Sun, *Nat. Commun.*, 2015, **6**, 7493.
- 22 H. Wang, Z. Lu, S. Xu, D. Kong, J. J. Cha, G. Zheng, P. C. Hsu, K. Yan, D. Bradshaw, F. B. Prinz and Y. Cui, *Proc. Natl. Acad. Sci. U. S. A.*, 2013, **110**, 19701–19706.
- 23 J. Wu, G. Yue, Y. Xiao, M. Huang, J. Lin, L. Fan, Z. Lan and J. Y. Lin, *ACS Appl. Mater. Interfaces*, 2012, **4**, 6530–6536.
- 24 W. Han, Z. Liu, Y. Pan, G. Guo, J. Zou, Y. Xia, Z. Peng, W. Li and A. Dong, *Adv. Mater.*, 2020, **32**, 2002584.
- 25 H. Zhou, J. Guo, C. Wang, X. Liu, S. Shi, J. Wei, X. Pu, W. Li, D. Zhang, J. Wang, X. Ren, H. Ma, X. Shao, X. Wei, J. Zhao, J. Yin and X. Zhang, *Adv. Mater. Interfaces*, 2019, **6**, 1801657.
- 26 J. Yin, J. Wei, J. Guo, S. Shi, N. Chai, K. Zhang, W. Xu, C. Yuan, T. Liu, W. Lin, Q. Zhang, H. Zhou, Y. Zhang, B. Chen, X. Pu, W. Li and X. Zhang, *ChemSusChem*, 2019, **12**, 795–800.
- 27 J. Xie, H. Zhang, S. Li, R. Wang, X. Sun, M. Zhou, J. Zhou, X. W. Lou and Y. Xie, *Adv. Mater.*, 2013, **25**, 5807–5813.
- 28 H. Wang, Z. Lu, D. Kong, J. Sun, T. M. Hymel and Y. Cui, *ACS Nano*, 2014, **8**, 4940–4947.
- 29 X. Geng, W. Wu, N. Li, W. Sun, J. Armstrong, A. Al-hilo, M. Brozak, J. Cui and T.-P. Chen, *Adv. Funct. Mater.*, 2014, **24**, 6123–6129.
- 30 H. Wang, D. Kong, P. Johannes, J. J. Cha, G. Zheng, K. Yan, N. Liu and Y. Cui, *Nano Lett.*, 2013, **13**, 3426–3433.
- 31 L. Li, J. Yan, T. Wang, Z. J. Zhao, J. Zhang, J. Gong and N. Guan, *Nat. Commun.*, 2015, **6**, 5881.
- 32 M. Chandra and D. Pradhan, *ChemSusChem*, 2020, **13**, 3005–3016.
- 33 S.-Y. Tai, C.-J. Liu, S.-W. Chou, F. S.-S. Chien, J.-Y. Lin and T.-W. Lin, *J. Mater. Chem.*, 2012, **22**, 24753.
- 34 G. Yue, J. Wu, Y. Xiao, M. Huang, J. Lin and J.-Y. Lin, *J. Mater. Chem. A*, 2013, **1**, 1495–1501.
- 35 M. Zheng, J. Huo, Y. Tu, J. Wu, L. Hu and S. Dai, *Electrochim. Acta*, 2015, **173**, 252–259.
- 36 W. Wang, X. Pan, W. Liu, B. Zhang, H. Chen, X. Fang, J. Yao and S. Dai, *Chem. Commun.*, 2014, **50**, 2618–2620.
- 37 S.-L. Chen, A.-C. Xu, J. Tao, H.-J. Tao, Y.-Z. Shen, L.-M. Zhu, J.-J. Jiang, T. Wang and L. Pan, *Green Chem.*, 2016, **18**, 2793–2801.
- 38 S. Hussain, S. A. Patil, A. A. Memon, D. Vikraman, B. A. Naqvi, S. H. Jeong, H.-S. Kim, H.-S. Kim and J. Jung, *Sol. Energy*, 2018, **171**, 122–129.
- 39 M. Xu, W. Wang, Y. Zhong, X. Xu, J. Wang, W. Zhou and Z. Shao, *J. Mater. Chem. A*, 2019, **7**, 17489–17497.
- 40 J. Yin, H. Zhou, Z. Liu, Z. Nie, Y. Li, X. Qi, B. Chen, Y. Zhang and X. Zhang, *ACS Appl. Mater. Interfaces*, 2016, **8**, 5314–5319.
- 41 H. Zhou, J. Yin, Z. Nie, Z. Yang, D. Li, J. Wang, X. Liu, C. Jin, X. Zhang and T. Ma, *J. Mater. Chem. A*, 2016, **4**, 67–73.
- 42 X. Wei, Y. Li, W. Xu, K. Zhang, J. Yin, S. Shi, J. Wei, F. Di, J. Guo, C. Wang, C. Chu, N. Sui, B. Chen, Y. Zhang, H. Hao, X. Zhang, J. Zhao, H. Zhou and S. Wang, *R. Soc. Open Sci.*, 2017, **4**, 171409.
- 43 Y. Li, J. Yin, C. Chu, N. Sui, S. Shi, J. Wei, F. Di, J. Guo, C. Wang, W. Xu, K. Zhang, X. Li, T. Guo, B. Chen, Y. Zhang, D. Wei, H. Hao, X. Wei, X. Zhang, J. Zhao, H. Zhou and S. Wang, *RSC Adv.*, 2018, **8**, 4340–4347.
- 44 S. Hussain, S. F. Shaikh, D. Vikraman, R. S. Mane, O.-S. Joo, M. Naushad and J. Jung, *RSC Adv.*, 2015, **5**, 103567.
- 45 C. Yu, X. Meng, X. Song, S. Liang, Q. Dong, G. Wang, C. Hao, X. Yang, T. Ma, P. M. Ajayan and J. Qiu, *Carbon*, 2016, **100**, 474–483.
- 46 W. Wang, Y. Wang, C. Li, Y. Wu, D. Zhang, K. Hong and Y. Sun, *Chem. Commun.*, 2017, **53**, 5461–5464.
- 47 X. Liu, X. Li, M. An, Y. Gao, Z. Cao and J. Liu, *Electrochim. Acta*, 2020, **351**, 136249.